Case Studies in Thermal Engineering 57 (2024) 104280

Contents lists available at ScienceDirect

Case Studies in Thermal Engineering

journal homepage: www.elsevier.com/locate/csite

Analysis of NePCM melting flow inside a trapezoidal enclosure with hot cylinders: Effects of hot cylinders configuration and slope angle

Nidhal Ben Khedher [a, b], S.A.M. Mehryan [c, **], Mohammad Shahabadi [d], Amira M. Hussin [e], Abed Saif Alghawli [f], Mohsen Sharifpur [g, h, i, *]

[a] Department of Mechanical Engineering, College of Engineering, University of Ha'il, 81451, Ha'il City, Saudi Arabia
[b] Laboratory of Thermal and Energetic Systems Studies (LESTE) at the National School of Engineering of Monastir, University of Monastir, Tunisia
[c] Young Researchers and Elite Club, Yasooj Branch, Islamic Azad University, Yasooj, Iran
[d] School of Aerospace and Mechanical Engineering, University of Oklahoma, Norman, OK, 73019, USA
[e] Department of Mathematics, Al-Aflaj College of Science and Humanities, Prince Sattam Bin Abdulaziz University, Al-Aflaj, 710-11912, Saudi Arabia
[f] Department of Computer Science, Al-Aflaj College of Science and Humanities, Prince Sattam Bin Abdulaziz University, Al-Aflaj, 710-11912, Saudi Arabia
[g] Department of Mechanical and Aeronautical Engineering, University of Pretoria, Pretoria, 0002, South Africa
[h] School of Mechanical, Industrial and Aeronautical Engineering, University of the Witwatersrand, Private Bag 3, Wits, 2050, South Africa
[i] Department of Medical Research, China Medical University Hospital, China Medical University, Taichung, Taiwan

ARTICLE INFO

Keywords:
NePCM
Trapezoidal enclosed medium
Adaptive mesh refinement
Hot cylinders
Melting flow

ABSTRACT

Hot cylinders within the cavity can find diverse thermal applications, ranging from electronic devices and heat exchangers to solar systems, nuclear reactors, and the thermal design of passive cooling systems. Consequently, considering the use of phase change materials (PCM) close to hot cylinders emerges as a viable method for both cooling and storing thermal energy. In this work, two hot cylinders are arranged vertically and horizontally in the nano-enhanced phase change material (NePCM) trapezoidal enclosure with varying angles. The novelty of the current study lies in the fact that no prior research has explored the impact of hot cylinders arrangement on the melting process of a NePCM within a trapezoidal cavity, considering various inclination angles. The fixed grid, adaptive mesh refinement, and enthalpy-porosity method are used to model the melting flow. The numerical results indicate that the trapezoidal enclosure with vertically arranged hot cylinders exhibits better thermal performance than the other configuration. It is also found that the full melting time for both arrangements is minimum when the angle of the trapezoidal enclosure is $\gamma = +40^{\circ}$. The reduction in full melting times for the vertical and horizontal arrangements of this angle are 25.3% and 29.6%, respectively, compared to the trapezoidal enclosure with $\gamma = 0.0^{\circ}$. Moreover, the NePCM with the graphite nanoplatelets (GNPs) of $\varphi = 1.0\%$ has the shortest melting time for $0.0\% \leq \varphi \leq 3.0\%$. As future research, further exploration into the complexities of non-Newtonian NePCM flow can be pursued. Additionally, there is potential to explore modifying the cylinders' geometry into elliptical forms, encompassing a range of aspect ratios.

* Corresponding author. Department of Mechanical and Aeronautical Engineering, University of Pretoria, Pretoria, 0002, South Africa.
** Corresponding author. Young Researchers and Elite Club, Yasooj Branch, Islamic Azad University, Yasooj, Iran.
E-mail addresses: alal171366244@gmail.com (S.A.M. Mehryan), mohsen.sharifpur@up.ac.za (M. Sharifpur).

https://doi.org/10.1016/j.csite.2024.104280
Received 19 February 2023; Received in revised form 9 December 2023; Accepted 17 March 2024
Available online 4 April 2024

Nomenclature

Latin symbols

A_m	Constant mushy parameter
$a(T)$	Step function
C_p	Sensible heat capacity ($J.Kg^{-1}.K^{-1}$)
f_{b_i}	Gravity-buoyancy force ($N.m^{-3}$)
f_{m_i}	Sink term of momentum equation ($N.m^{-3}$)
g	Gravity acceleration ($m.s^{-2}$)
H	Height of the trapezoidal cavity (m)
k	Thermal conductivity ($W \cdot m^{-1} \cdot K^{-1}$)
$PFP(T)$	phase-field parameter
p	Pressure (Pa)
R	Radius of hot cylinders (m)
T	Temperature (K)
t	Time (s)
u	x-velocity component ($m.s^{-1}$)
v	y-velocity component ($m.s^{-1}$)
x,y	Cartesian coordinates (m)

Greek symbols

β	Thermal expansion coefficient (K^{-1})
γ	Trapezoidal cavity angle (°)
ΔT_f	Melting temperature window (K)
ϵ	Numerical constant
μ	Dynamic viscosity ($Pa.s$)
ρ	Density ($kg.m^{-3}$)
φ	Mass fraction of nanoparticles

Subscripts

f	Fusion temperature
h	Hot wall
LNePCM	Liquid nano-enhanced phase change material
NePCM	Nano-enhanced phase change material
SNePCM	Solid nano-enhanced phase change material

1. Introduction

Enhancing the efficiency of heat dissipation in electronic devices [1], air conditioning and refrigeration systems [2], automotive technologies [3], solar collector setups [4], and heat sinks [5] is increasingly imperative to ensure effective thermal regulation. Furthermore, the heat transfer process plays a crucial role in influencing the overall quality of the investigated processes. Phase change materials (PCMs) have captured the attention of scientists and engineers as a promising solution to address this challenge [6]. Due to their exceptional thermal properties and the capacity to store and release thermal energy during phase transitions, PCMs are attracting significant interest across a broad spectrum of applications. These applications include solar thermal collectors [7], solar cells [8], passive building conditioning [9], and electronic systems [10], all benefiting from the remarkable potential of PCMs. While phase PCMs offer various advantages, a fundamental drawback associated with these materials is their relatively low thermal conductivity. This limitation diminishes the efficiency of heat transfer during both the melting and solidification phases. To overcome this constraint of PCMs, numerous methods to enhance heat transfer have been devised. These approaches include the use of fins [11], metal/graphite matrices [12], heat pipes [13], loadings high-conductivity nanoparticles in the PCM [14], and nano/micro-encapsulation of PCM [15].

Based on the findings of the literature review, it is observed that PCMs are primarily contained within sealed enclosure modules. Consequently, investigating the melting behavior of PCMs within enclosure has emerged as a highly intriguing research topic, garnering growing interest from researchers. Especially, when hybrid enhancement techniques like fins [16], metal porous foam [12] and nanoparticles dispersion [14] are used. Kamkari et al. [17] extensively addressed both experimental and computational investigations concerning the phase change behavior of a PCM within a rectangular cavity. A number of recent studies have directed their attention towards the dynamic process of melting, taking into account the influence of heat transfer through advection.

In [18], the natural convection of molten PCM in a rectangular container may contribute to cool photovoltaic (PV) panels. After melting, the heat transmission capability of the PCM container's fins is assessed. When the same type of enclosure is evaluated, the average Nusselt number is larger with higher aspect ratios. According to the findings of this investigation, although fins shorten the PCM melting period, they may slow down natural convection heat transfer in molten PCM. Thus, in systems like PV/PCM, careful study is

required to maximize natural convection benefits. Ahmed et al. [19] investigated experimentally and numerically the phase change of paraffin wax inside a trapezoidal aluminum enclosure. They showed that using fins allows a time saving of 28% compared to pure PCM in unfinned latent heat thermal energy storage systems.

Cesaro Oliveski et al. [20] investigated the phase change flow of lauric acid inside a finned rectangular enclosure while maintaining the total area of fin and mass of the PCM constant, hence modifying just the fin aspect ratio. A parametric investigation of 78 alternative fin designs was used to perform the investigation. The fin dimensions were modified within a predetermined range of area fraction and width combinations. The evaluated fins were a mix of 9 fin aspect ratios and 9 fin-to-cavity area fractions. They discovered that increasing the fin length and, as a result, lowering the fin aspect ratio reduces the overall duration of the melting process in all investigated scenarios.

Adding nanoparticles to fluids and materials is a process that has gained a lot of attention in various fields due to the unique properties and potential benefits that nanoparticles can offer [21–23]. Nanoparticles are particles with dimensions in the nanometer scale, typically ranging from 1 to 100 nm. They can be engineered from a wide range of materials, such as metals, metal oxides, polymers, and more, each with its own specific properties [24–26]. Dhaidan et al. [27] reviewed numerical and experimental research on the solidification of nano-enhanced PCM (NePCM) in various typical cavities. Mehryan et al. [28] studied the influence of using a porous medium layer and NePCM on the heat transmission enhancement in an enclosure. They found that a porous layer might significantly improve the heat transmission and thermal behavior of NePCM.

Geometries and orientations of PCM containers highly affect heat transmission in PCM rectangular cavities [29]. According to the literature, there are numerous approaches for enhancing the thermal conductivity of the PCM. However, there have been fewer studies on the impact of enclosure shape and orientation on PCM thermal performance. Meng et al. [30] studied the influence of inclination angle on the thermal behavior of PCM in a cavity filled with copper foam fins. For the thermal storage unit, twelve inclinations ranging from 0° to 360° were investigated. The liquid fraction, temperature response rate, and average heat flow were used as assessment metrics.

Sathe and Dhoble [31] investigated the melting flow of a PCM inside a rectangular finned enclosure with a heated top and a fin at the bottom. The goal of the research was to increase melting time and reduce solidification time. The enclosure was tilted at several angles with different fin numbers and PCM thicknesses. To investigate the melting rate, the enclosure was tilted at $\pi/6$, $\pi/4$, $\pi/3$, and $\pi/2$ with PCM thicknesses of 2, 3, and 4 cm, respectively. Korti et al. [32] conducted an experiment to investigate the influence of tilt on the thermal behavior of PCM melting in a square cavity.

The existence of hot cylinders inside the cavity might have a variety of thermal applications, including electronic devices, heat exchangers, solar systems, nuclear reactors, and thermal design of passive cooling systems and others. Recently, Selimefendigil et al. [33] studied numerically the mixed convection in a PCM-filled cavity with an adiabatic rotating cylinder. It was discovered that the cylinder's angular rotating speed, vertical placement, and size might be utilized to regulate the heat transmission and melting process in the cavity. Furthermore, they found that the average Nusselt number increases with the angular speed.

According to a literature review, the study of trapezoidal cavities englobing NePCM and heated cylinders is still a promising field for further research. The novelty of the present work is that no study has investigated the effect of the arrangement of hot cylinders on the melting process of a NePCM inside a trapezoidal cavity with different inclination angles. Broadly speaking, this study aims to address the following inquiries.

- What impact does the configuration of the heated cylinders have on the melting rate, heat transfer rate, temperature distribution, and velocity patterns in the NePCM trapezoidal enclosure?
- How does the angle of the trapezoidal cavity affect melting characteristics, including melting rate, heat transfer rate, temperature distribution, and velocity field?
- What impact does the dispersion of graphite nanoplates within the PCM have on heat transfer and melting rates, as well as the governing fields?

2. Problem description

Fig. 1 illustrates two different configurations of closed trapezoidal mediums, both of which are initially filled with a solid PCM. The hot cylinders are maintained at a high temperature of T_h, which is higher than the melting temperature of the PCM. The outer walls are well insulated. In both configurations, the angle of the trapezoid, denoted as γ, varies from -40° to $+40^\circ$. For this study, 1-Tetradecanol serves as the base PCM, while graphite nanoplatelets (GNPs) act as the dispersed nano-sized particles. The thermophysical characteristics of the NePCM for different mass fractions of nanoplates, obtained experimentally [34], are tabulated in Table 1. The volume of NePCM is considered as a constraint. When $\gamma = 0.0^\circ$, the width and height of the enclosure are $H = 50mm$. The radius of the hot cylinders is $R = 0.1H$.

3. Mathematical formulation

To capture the phase change flow of the NePCM, the enthalpy-porosity technique is applied, and a fixed grid with adaptive mesh refinement (AMR) is provided for the computational domain. The enthalpy-porosity method has found extensive application in studying solidification-melting phenomena within containers, especially when natural convection plays a significant role. This method boasts two primary advantages: rapid convergence and high accuracy. Based on the enthalpy-porosity method, the NePCM domain is divided into three distinct zones: fluid, solid, and the intermediate region known as the mushy zone. Also, these three sub-domains are distinguished by the temperature of melting, i.e., T_f, and the melting temperature window, i.e., ΔT_f. The mushy zone, character-

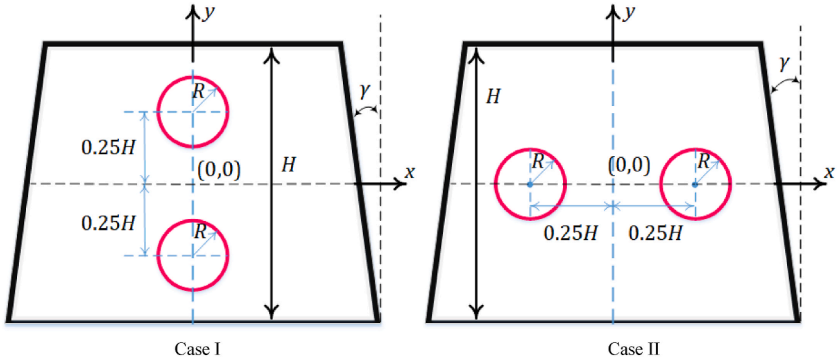

Fig. 1. Schematic view of the two studied configurations.

Table 1
Thermophysical properties of the NePCM at different mass fractions of GNPs [34].

Properties	0.0 wt%	0.50 wt%	1.0 wt%	3.0 wt%
Density (solid)	891.4	894.1	896.9	907.9
Density (liquid)	821.6	824.3	826.9	837.6
Dynamic viscosity	13.23	23.45	59.5	194.01
Specific heat capacity (solid)	2040	2020	1990	1910
Specific heat capacity (Liquid)	2360	2330	2300	2190
Melting point	37	37	37	37
Latent heat	227.8	219.5	212.2	183.5
Thermal expansion coefficient	0.001018	0.001018	0.001008	0.000987
Thermal conductivity (solid)	0.252	0.350	0.451	0.540
Thermal conductivity (liquid)	0.159	0.180	0.260	0.320

ized by its porous structure containing both liquid and solid phases, exhibits a velocity field with significant gradients. The enthalpy-porosity method can integrate the concept of AMR to enhance computational efficiency and solution accuracy. AMR constitutes a dynamic mesh adjustment strategy, wherein the grid resolution is selectively refined based on the evolving characteristics of the solution. In the context of the enthalpy-porosity method, which addresses processes involving solid-liquid phase changes, AMR proves instrumental in optimizing computational resources. Throughout the simulation, specific regions of interest may undergo substantial variations in temperature, phase transitions, or other relevant parameters. The adaptive refinement feature of AMR facilitates an intensified grid resolution in these critical zones while maintaining a coarser mesh in less dynamically active regions.

The AMR strategy serves as a judicious allocation of computational resources, directing heightened attention to areas of the simulation where intricate changes unfold. By dynamically refining the mesh in response to evolving solution features, AMR significantly contributes to both the precision and computational efficiency of the enthalpy-porosity method. This tailored refinement approach ensures a focused utilization of computational resources, thereby elevating the method's efficacy in capturing the intricacies inherent in solidification-melting processes.

To comprehensively address the presented problem, the following assumptions are being considered: 1) During the phase change flow, the volume change of the NePCM is ignorable [17]; 2) The flow of melted liquid is laminar, incompressible, and Newtonian; 3) The dispersion of GNPs within the PCM is uniform, and there is no tendency for the GNPs to settle; 4) The Boussinesq approximation, applied in the current work, simplifies the mathematical description of fluid flows by allowing researchers to neglect density variations in most parts of the equations, focusing only on buoyancy-driven effects caused by temperature differences [29]. Considering the assumptions mentioned above, the continuity, momentum, and energy equations of the domain containing NePCM can be formulated as.

I) Continuity [35].

$$\frac{\partial u_j}{\partial x_j} = 0 \tag{1}$$

II) Momentum conservation [36,37].

$$\rho_{LNePCM}\left(\frac{\partial u_i}{\partial t} + u_j\frac{\partial u_i}{\partial x_j}\right) = -\frac{\partial p}{\partial x_i} + \mu_{LNePCM}\frac{\partial^2 u_i}{\partial x_j x_j} + f_{b_i} + f_{m_i} \tag{2}$$

where $x_1 = x$, $x_2 = y$, $u_1 = u$, and $u_2 = v$. The sink term of the momentum equation (f_{m_i}), demonstrating zero value of velocity within the solid region of the NePCM can be written as the following [36]:

$$f_{m_i} = -\frac{A_m(1-a(T))^2}{a^3(T)+\epsilon}u_i \tag{3}$$

In Eq. (3), A_m is a constant value of $A_m = 5\times10^5 kgm^{-3}s$, that is large to make the velocity vector of zero for the solid region of the PCM. Another parameter, ϵ, is set to a very small fixed value ($\epsilon = 0.001$) to prevent the denominator from being zero. In Eq. (3), $a(T)$ is a ramp function, expressed by:

$$a(T) = \begin{cases} 0 & T \le T_f - \Delta T_f/2 \\ \dfrac{T-T_f}{\Delta T_f} + \dfrac{1}{2} & T_f - \Delta T_f/2 < T < T_f + \Delta T_f/2 \\ 1 & T \ge T_f + \Delta T_f/2 \end{cases} \tag{4}$$

The buoyancy term of the momentum equation by applying the Boussinesq approximation is:

$$f_{b_i} = -\rho_{LNePCM}\beta_{LNePCM}g_i = -\rho_{LNePCM}\beta_{LNePCM}\begin{cases} 0 & i=1 \\ g & i=2 \end{cases} \tag{5}$$

III) Energy conservation [36,37].

$$\rho_{NePCM}C_{p,NePCM}\frac{\partial T}{\partial t} + \rho_{LNePCM}C_{p,LNePCM}u_j\frac{\partial T}{\partial x_j} = \frac{\partial}{\partial x_j}\left(k_{NePCM}\frac{\partial T}{\partial x_j}\right) - \rho_{NePCM}L_{NePCM}\frac{\partial a(T)}{\partial t} \tag{6}$$

in which,

$$k_{NePCM} = k_{SNePCM} + a(T)\left(k_{LNePCM} - k_{SNePCM}\right) \tag{7}$$

$$\rho_{NePCM} = \rho_{SNePCM} + a(T)\left(\rho_{LNePCM} - \rho_{SNePCM}\right) \tag{8}$$

$$\rho_{NePCM}C_{p,NePCM} = \rho_{SNePCM}C_{p,SNePCM} + a(T)\left(\rho_{LNePCM}C_{p,LNePCM} - \rho_{SNePCM}C_{p,SNePCM}\right) \tag{9}$$

4. Numerical approach, grid sensitivity analysis, and code verification

4.1. Numerical approach

To numerical modeling, the enthalpy-porosity accompanied by an adaptive refinement grid has been employed for the present study. As mentioned before, a sink term, i.e. $f_{m_i} = -\frac{A_m(1-a(T))^2}{a^3(T)+\epsilon}u_i$, is established within the momentum equation to ensure a velocity of zero in the solid region of the NePCM. In the equation that keeps track of energy conservation, we include a heat sink term, i.e. $-\rho_{NePCM}L_{NePCM}\frac{\partial a(T)}{\partial t}$. This term measures how much energy is used up when melting happens in a certain amount of space. To capture and analyze the steep changes in variables within the mushy zone, the method of adaptive mesh refinement is employed to generate a high-quality grid. To discretize the nonlinear differential equations and implement user-defined codes, COMSOL Multiphysics software has been utilized. In this regard, Galerkin finite element method was employed to solve the governing equations [38]. A first-order interpolation function has been employed for the main parameters of v_i, p, T, among the points.

A phase-field parameter, denoted as $PFP(T)$, is introduced to establish bounds for the mesh adaptation domain. Regarding the temperature gradient, the adaptive mesh employs a temperature window equal to $1.5\Delta T_f$, whereas this window is ΔT_f for the mushy zone. The temperature window of the adaptive mesh facilitates the generation of a finer mesh in the region that is slightly thicker than the mushy strip, while a coarser mesh is created in the remaining parts of the computational domain. $PFP(T)$ is expressed as follows:

$$PFP(T) = \begin{cases} 0 & T \le T_f - \dfrac{3\Delta T_f}{2} \\ 1 & T_f - \dfrac{3\Delta T_f}{2} < T < T_f + \dfrac{3\Delta T_f}{2} \\ 0 & T \ge T_f + \dfrac{3\Delta T_f}{2} \end{cases} \tag{10}$$

A free step Backward Differentiation Formula and a floating time step are used to regulate the time increment, with a maximum value set at 0.2 s. Ensuring the stability of the provided code by shorter time steps, specifically during the primary times, can be achieved by considering changeable time steps. The minimum time step used by the solver in this study is around 10^{-4} s. To solve the residual equations, PARallel DIrect SOlver has been employed with a Newtonian damping factor of 0.8 [39,40], and the iterations continues to satisfy the residual error of O (10^{-6}).

4.2. Grid sensitivity analysis

Fig. 2 (a) shows the adaptive mesh in three different time steps for the cylinders' horizontal and vertical arrangements. It can be seen a smooth transition of grids from the first time step ($t = 2000s$) towards the last one ($t = 8000s$) for both horizontal and vertical arrangements.

A quality grid needs to be provided to achieve precise numerical outcomes. So, in the case of grid independency, four grids of different sizes of 5004, 16,805, 23,099, and 30,852 have been provided (Fig. 2 (b)). The triangular type of grids is used to discretize the equations inside NePCM domain study. The melted volume fraction (MVF) is the variable chosen for the comparison among different grids. No considerable difference between the chosen grids can be seen, especially grid cases 2, 3, and 4. Therefore, the second grid containing 16,805 elements has been selected for the simulations to reduce the computational cost and times.

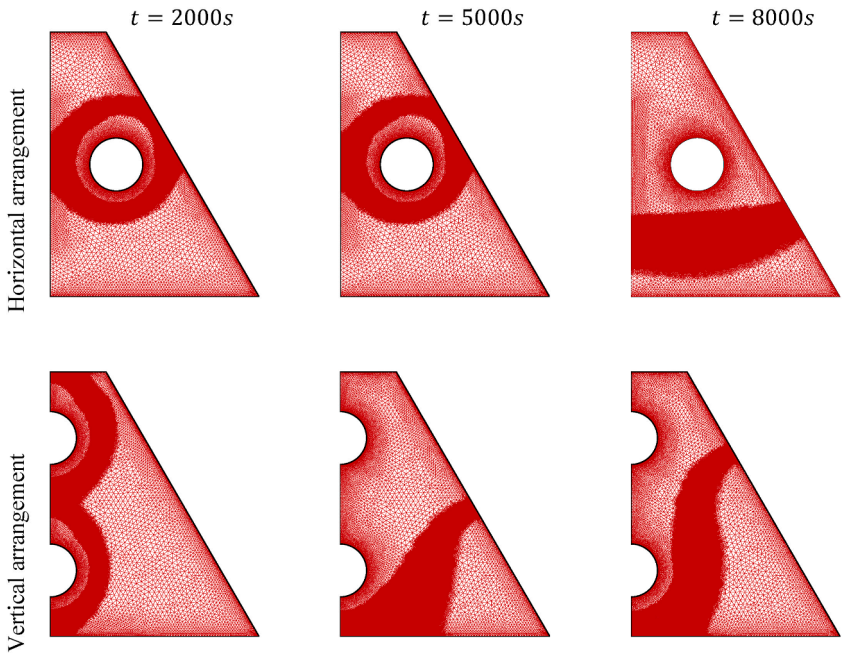

Fig. 2 (a). Adaptive mesh history for the horizontal and vertical arrangements of the hot cylinders.

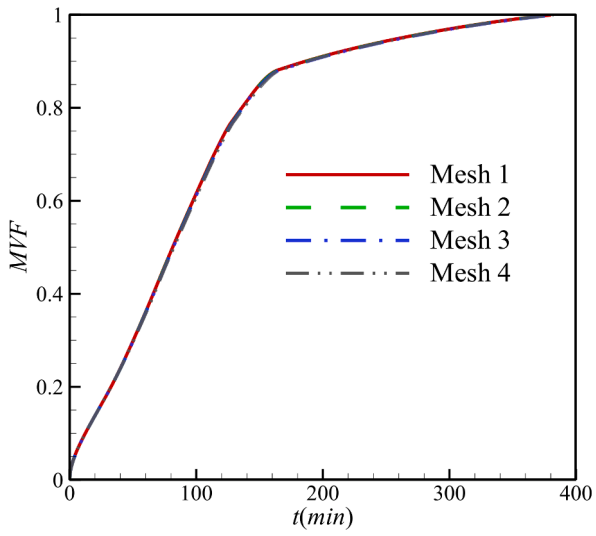

Fig. 2 (b). Dependency of the MVF on the mesh size.

4.3. Code verification

Previous numerical and experimental research has been examined as validation cases to check the accuracy and correctness of the results. The numerical and experimental study conducted by Kamkari et al. [17], which investigated the melting process of the PCM within a rectangular cavity, has been selected for the validation case. The results of this research and those of Ref. [17] are shown in Fig. 3 (a). The validating phase change fields are shown at two times: 30 min, and 60 min with $Ra = 8.3 \times 10^8$. A good agreement is evident among the results, confirming the accuracy of the present study.

As the second verification, the average Nusselt numbers of the study conducted by Kim et al. [41] and those obtained by the current work are compared in Fig. 3 (b). Kim et al. [41] analyzed the natural convection flow of air in a square cavity having a hot cylinder. The δ parameter is the deviation of the cylinder from the center of the cavity.

5. Results and discussion

Fig. 4 (a) depicts the streamlines, melted PCM fields, and the velocity magnitude contours over time for three angles of the trapezoidal enclosure with the horizontal arrangements of the hot cylinders for different time steps. The volume of PCM in the upper portion of the cylinders within the cavities varies for different configurations. This variation can significantly affect the melting rate at various angles. For instance, at an angle of $\gamma = +30^{\circ}$, where the most PCM is located above the cylinders compared to $\gamma = 0^{\circ}$ and $\gamma = -30^{\circ}$, we observe the fastest melting time for the entire PCM due to the tendency of the hot melted PCM to move upward. At the primary time steps ($t = 2000s$) when the conductive heat transfer method is dominant, a thin melted layer of PCM is seen around the hot cylinders. At this time, small vorticities of the melted PCM are formed around the cylinders. Gathering of these small vorticities by improving the primary movements due to the natural convection enhancements during the time, the melting area and fluid PCM increase especially towards the upper part of the trapezoidal cavity. This is expected because of the buoyancy effects on the melted PCMs. At the following time snap ($t = 5000s$), the velocity contour shows a higher range of magnitude than the other times due to the dominancy of natural convection and movements of fluid, correspondingly. Afterwards ($t = 8000s$ and

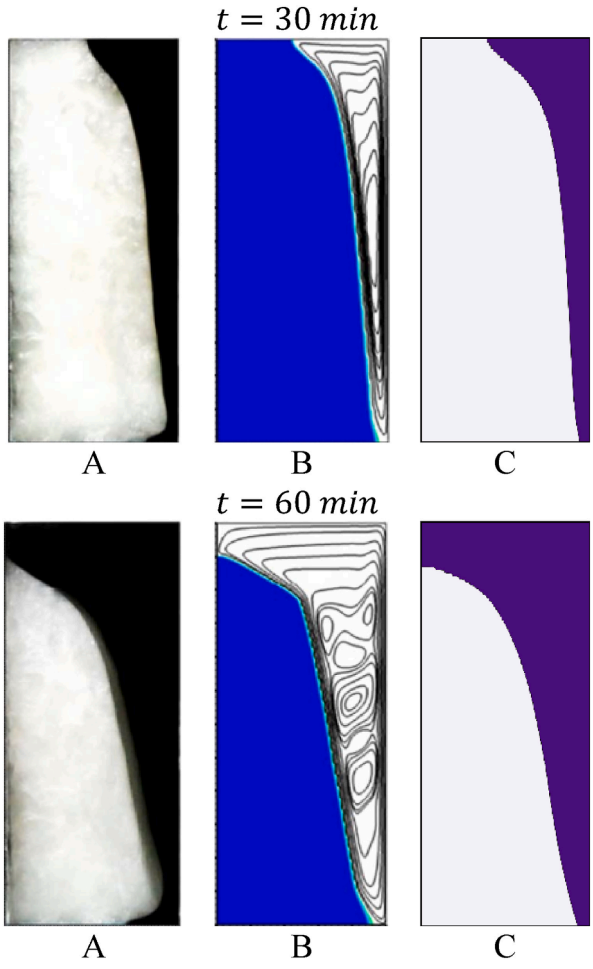

Fig. 3 (a). Comparison between the melting fields of the study conducted by Kamkari et al. [17] and the current study; A: experimental results of Ref. [17], B: numerical results of Ref. [17], and C: present work.

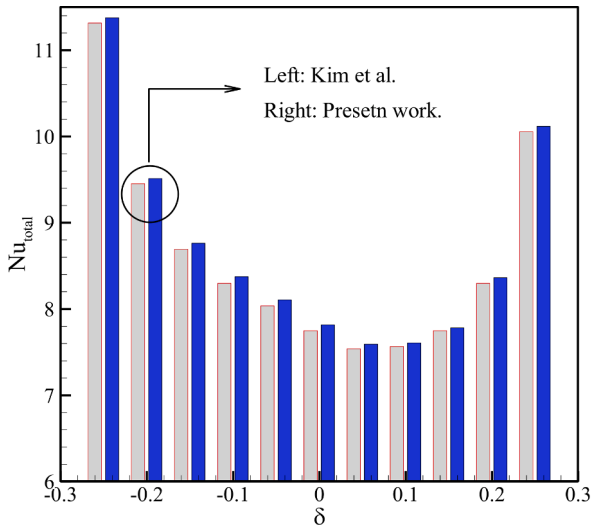

Fig. 3 (b). Average Nusselt number at the cylinder shell in comparison with numerical data of Kim et al. [41] for $Pr = 0.7$:

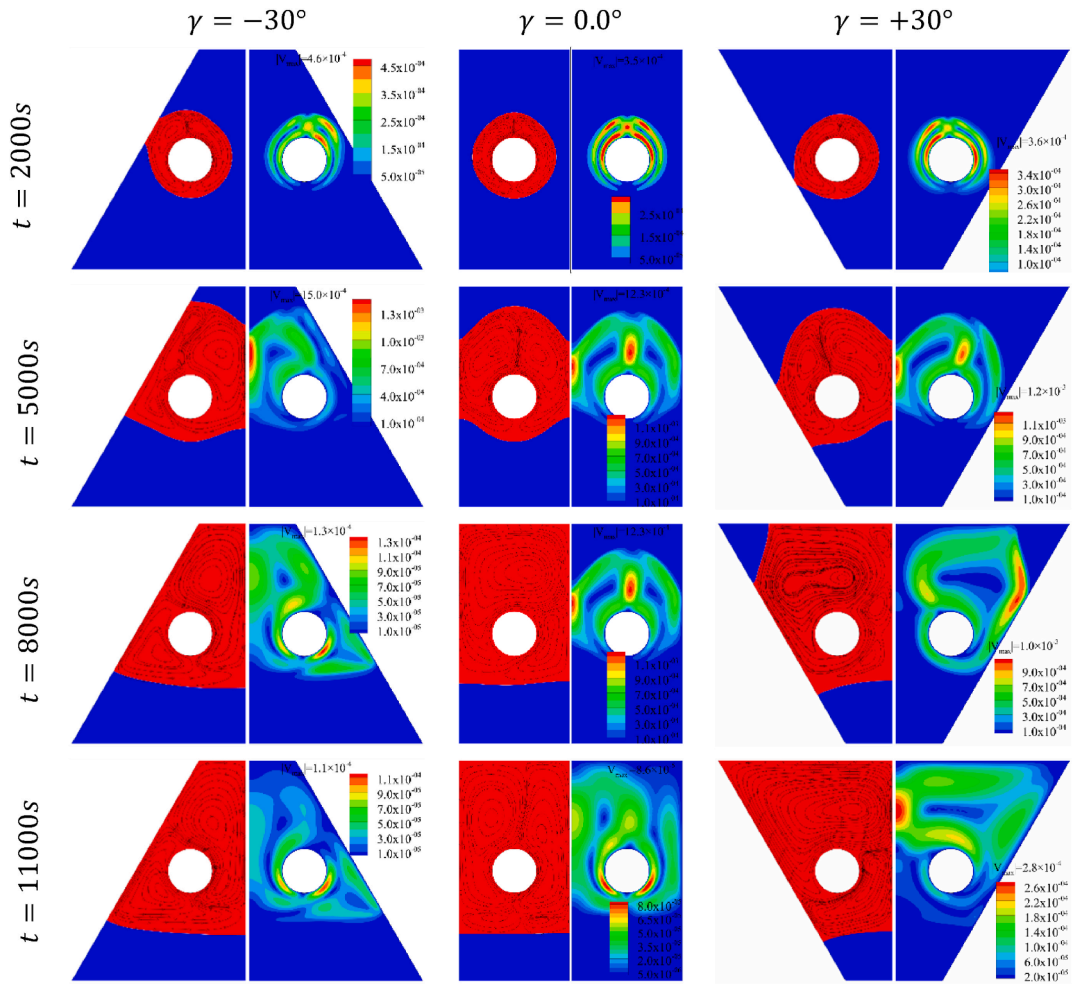

Fig. 4 (a). Dependency of the melting field, streamline patterns, and velocity magnitude field on the angle of trapezoidal enclosure with the horizontal arrangement of hot cylinders.

$t = 11000s$), as the whole of the PCM located in the upper zone has been melted and the temperature of this area increases, the strength of natural convection decreases, leading to the reduction of velocity magnitude. As PCM melts in the upper part of the cylinders, the heat from the cylinders further warms the melted liquid. Consequently, the temperature difference between the cylinders and the melted PCM decreases, resulting in a reduced flow velocity of the melted PCM. Larger vorticities are seen in streamline contours at these times ($t = 8000s$ and $t = 11000s$) because of more melted PCM created. There are two big vorticities formed above and beyond the cylinders for this configuration at the final time step ($t = 11000s$). In the case of velocity magnitude, both cavities of $\gamma = -30^{\circ}$ and $\gamma = +30^{\circ}$ have higher values compared to the case $\gamma = 0.0^{\circ}$. This is the result of inclined side walls that helps the variations in the direction of the melted flow movement and higher velocity magnitude. Between two cavities with inclined side walls, $\gamma = -30^{\circ}$ and $\gamma = +30^{\circ}$, the later one shows higher velocity magnitude in all times steps except the first one, when there is no considerable melted PCM. This is because in the cavity with a $\gamma = +30^{\circ}$, the wider area of melted PCM along with the side walls facilitate the movement of the molten liquid.

Fig. 4 (b) illustrates the dependency of the temperature field on the orientation of the cavity for three different angles of $\gamma = -30^{\circ}, \gamma = 0.0^{\circ}$, and $\gamma = -30^{\circ}$ for horizontal arrangements of the hot cylinders at various time shots. When the PCM close to hot cylinders reaches its melting point, $310\,K$, it starts melting. As said before, due to the dominancy of the natural convection in comparison to conductive term at the following times and the tendency of the fluid PCM to move upward in the cavity, the upper zone of cylinders experiences higher temperature within the cavity. After the temperature equivalency of the hot cylinders and their upper zone, at the final time snaps, it is seen higher temperature range for the bottom part of the cylinders as the PCM of that area starts melting by the hot cylinders and fluid above PCM. At the first time snap ($t = 2000s$), the cavity of the angle $\gamma = -30^{\circ}$ experiences the widest range of temperature variations from $306\,K - 320\,K$, while the configuration of $\gamma = 0.0^{\circ}$ has the temperature range of $309\,K - 318\,K$. Indeed, it can be stated that the temperature uniformity is greater in the trapezoidal cavity with a $\gamma = 0.0^{\circ}$. In the cavity with $\gamma = -30^{\circ}$, a smaller amount of PCM is located above the cylinders, leading to a faster melting process in this area. Subsequently, the heat from the cylinders is utilized to further raise the temperature of the liquid PCM. Conversely, a larger amount of PCM is situated in the lower region of this cavity, where the heat from the cylinders is stored as latent energy within the PCM, resulting in a lower temperature range. These conditions contribute to greater temperature non-uniformity within this cavity. At the final time shot, when most of the PCM has melted and the temperature equivalency happens between hot cylinders and the melted PCM, there is no significant difference in the temperature range within the cavity among all configurations.

Fig. 5 (a) shows the streamlines, melted PCM fields, and the velocity magnitude contours for three angles of the trapezoidal enclosure with the vertical arrangement of the hot cylinders in different time steps. Same as the horizontal arrangement of the cylinders, there is a small melting zone around the cylinders at the primary time steps. As time passes ($t = 5000s$), the melted area around both cylinders attaches together and forms large vorticity between the cylinders. The velocity experiences its maximum at the centerline of the cylinders at this time. In the vertical arrangement of cylinders, the maximum velocity is seen for $\gamma = +30^{\circ}$

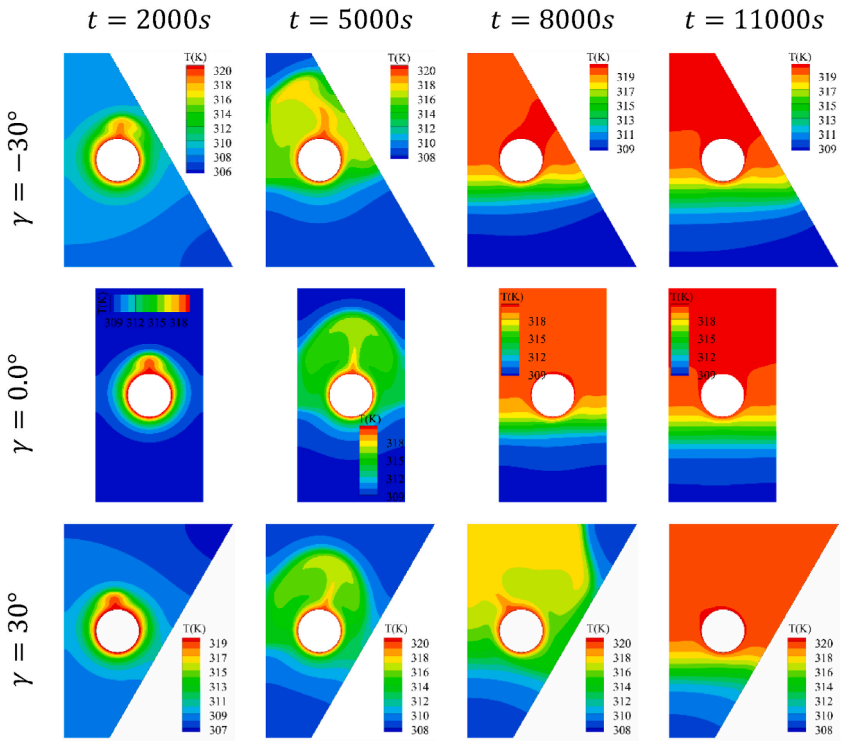

Fig. 4 (b). Dependency of the temperature fields on the angle of trapezoidal enclosure with the horizontal arrangement of hot cylinders.

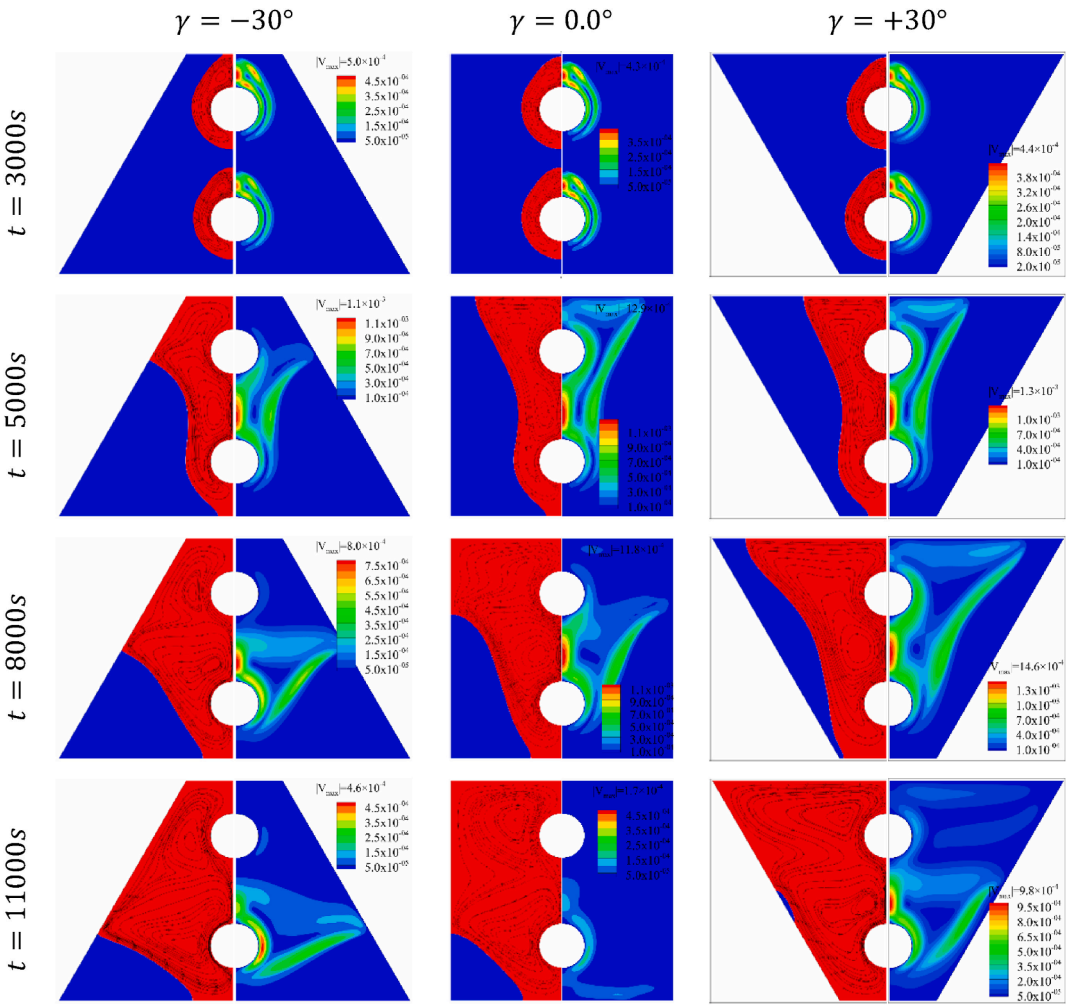

Fig. 5 (a). Dependency of the melting field, streamline patterns, and velocity magnitude field on the angle of trapezoidal enclosure with the vertical arrangement of hot cylinders.

same as the horizontal one, due to the wider area for melted PCM movements. At the final timestep (t = 11000s), the case γ = + 30° shows the maximum rate of melted PCM among the three cases. As previously mentioned, within the cavity with γ = + 30°, a substantial volume of PCM resides in the upper portion of the cavity. The upward motion of the hot fluid assists in melting this considerable volume of PCM. All three configurations of the trapezoidal cavity have two main vorticities formed next to the cylinders, and the bottom one is bigger. Also, the PCM flow velocity is higher next to the bottom cylinder as the melting phenomena around the upper one had been finished, and it is continuing toward the downer zone of the cavity. This can be attributed to the smaller temperature difference between the lower cylinder and the surrounding area.

Fig. 5 (b) indicates the temperature field for the vertical arrangement of the cylinders at different angles of the trapezoidal cavity in four time shots. Based on the conduction heat transfer by the hot cylinders at the primary time steps, the temperature of PCMs in the zone close to the cylinders increases. Subsequently, the PCM temperature reaches its melting point, initiating the formation of a natural convection flow. The upper part of the cavity experiences more increase in temperature compared to other regions. This is because the convective flow causes the hot PCM near the cylinders to rise and mix with the cooler PCM in the upper part of the cavity. As a result, the upper part heats up sooner. At different angles of the cavity, γ = 30° shows the lowest temperature range inside the cavity, as it has a larger volume of PCM at the upper part of cavity leading to longer heat transfer time around the whole of it by the convective term.

Fig. 6 (a) shows variations of the total Nusselt number versus time for different angles of trapezoidal cavity for both lower and upper cylinders in their vertical arrangement. Based on this figure, the heat transfer rate of the hot cylinders to the PCM inside the cavity can be evaluated. Before the melting start, the temperature difference between the hot cylinders and the PCM is significant, contributing to the high value of the Nusselt number at the primary time. This temperature difference reduces over time as the PCM around the cylinder reaches higher temperatures, so the Nusselt number starts falling. This trend is seen for both bottom and upper cylinders. As shown, for the lower cylinder when $t \geq 25$ *mins*, the Nusselt number increases, demonstrating the beginning of the natural convection heat transfer (Fig. 6 (a) (A)). Through the convective dominant time, the Nusselt number shows a relatively constant

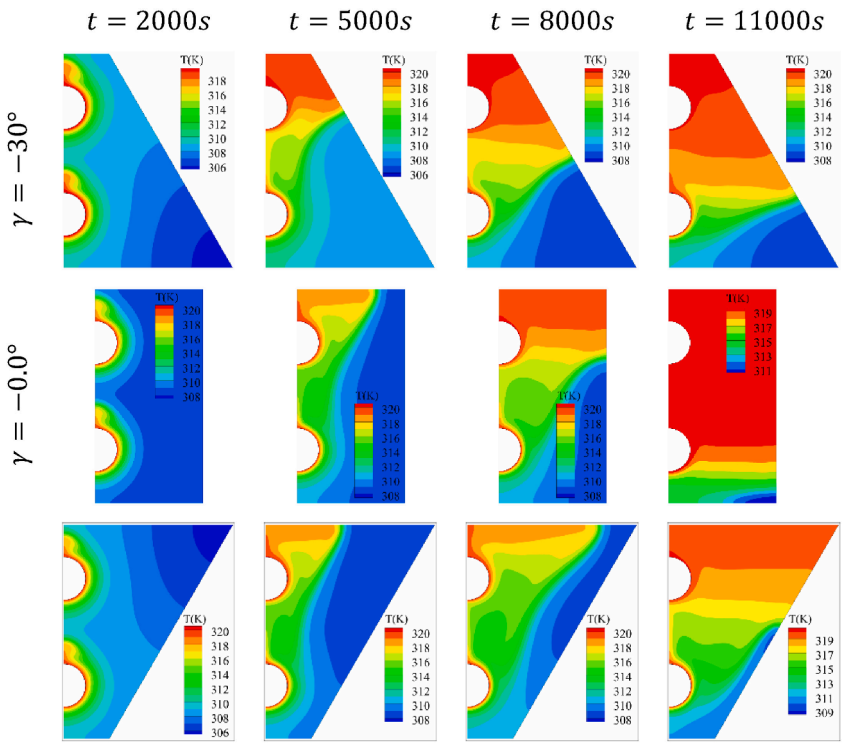

Fig. 5 (b). Dependency of the temperature fields on the angle of trapezoidal enclosure with the vertical arrangement of hot cylinders.

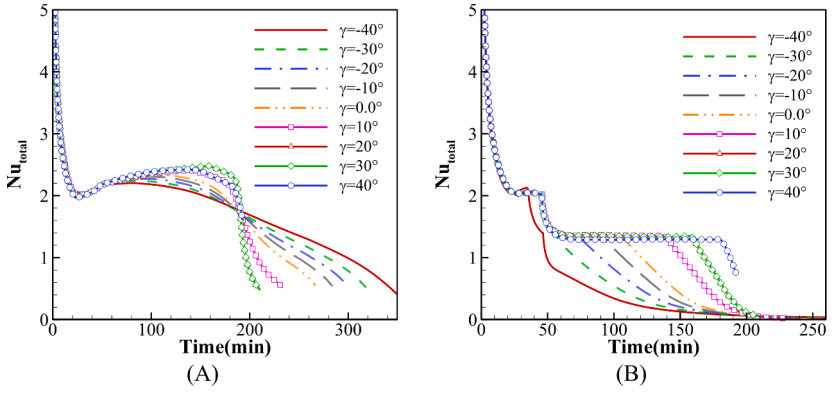

Fig. 6 (a). The effect of angle of the trapezoidal enclosure on the Nusselt numbers of the vertical arrangement of the hot cylinders; (A) lower cylinder, and (B) upper cylinder.

trend for the upper cylinder. After this time, the Nusselt number of the lower cylinder in all angles has downward trend. For the lower cylinder (Fig. 6 (a) (A)), all the graphs of positive angles of the cavity indicate approximately the same values, while the negative ones experience some variations. The same behavior of the Nusselt number is seen for the upper cylinder. There is a considerable difference in the Nusselt number trend for the negative angle configurations between upper and lower cylinders.

For the lower cylinder, after terminating of the positive effect of the convective heat transfer and relative temperature equivalency, by the start of decreasing in the Nusselt number, cavities with more negative inclined angles shows higher rate of the Nusselt number, while this is reversed for the upper cylinder; so that more negative inclination leads to the sharper decrease in the Nusselt number. For example, in Fig. 6 (a) (B), the cavity of $\gamma = -40^{\circ}$ has a small period of the constant Nusselt number and a sharp decrease afterwards. While at the same figure, $\gamma = -10^{\circ}$ experiences a more constant trend of the Nusselt number. Finally, at the end of the melting process, all liquid PCMs reach thermal equilibrium with the temperature of the hot cylinders leading to the final fall of the Nusselt number. The thermal equilibrium between the upper cylinder and the fluid PCM around it happens sooner when the melting process finishes at the upper part of the cavity as it was shown in Fig. 5 (a). The variation in the total Nusselt number of the different angles of trapezoidal cavity for both horizontal and vertical arrangement of hot cylinders is depicted in Fig. 6 (b). In the vertical case, Fig. 6 (b) (B), the positive angle configurations have a constant rate of the Nusselt number after the dominancy of the convection. Af-

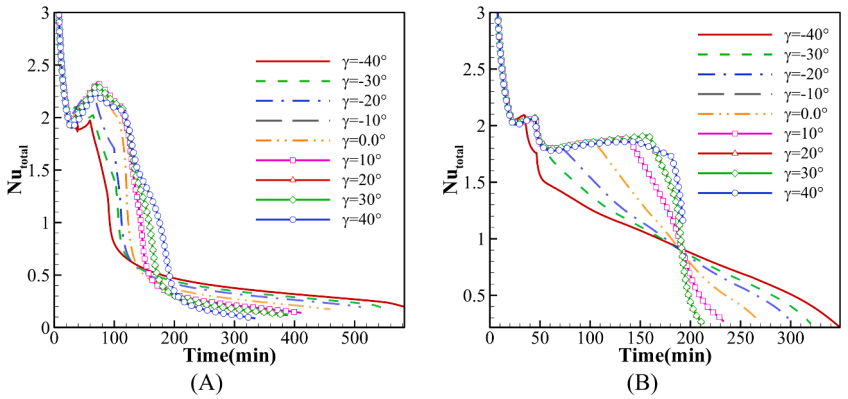

Fig. 6 (b). The effect of angle of the trapezoidal enclosure on the total Nusselt number; (A) horizontal arrangement of the hot cylinders, and (B) vertical arrangement of the hot cylinders.

terwards and due to the thermal equivalency of the melted hot PCM and the cylinders, the Nusselt number has a sharp fall. However, for Fig. 6 (a) (A), during the period of transition from the conductive term to the convective, a slightly increasing trend is seen for the Nusselt number. These changes in the slop of the Nusselt number lead to the final fall based on the thermal equilibrium. The vertical arrangement of the cylinders demonstrates an earlier time of complete melting of the PCM, and the negative angle configurations of trapezoidal cavity have a longer time of melting as expected because of the higher volume of the PCMs under hot cavities. The positive angles of the vertical cylinder arrangement reach the fully melting and the thermal equivalency leading to relatively zero Nusselt number after around $t = 200\ min$, while this time for horizontal configurations is around $t = 300\ min$. For the negative cases, the vertical arrangement of the cylinders experiences the whole melting around $t = 200\ min$ sooner than the horizontal one.

Fig. 7 (a) illustrates the MVF variations versus time and the total melting time for different angles of trapezoidal cavity at both horizontal and vertical arrangements of the cylinders. It can be seen that at the primary time steps, when only the conductive mechanism is dominant and the melting process only occurs at a small area close to the hot cylinders for both horizontal and vertical arrangements, MVF graph shows the same trend and increases in a constant slope. After this time, for the vertical arrangement of the cylinders, Fig. 7 (a) (B), the cavity angle of $\gamma = 40^{\circ}$ keeps its trend up to the time around $t = 200\ min$, when the whole PCM melts.

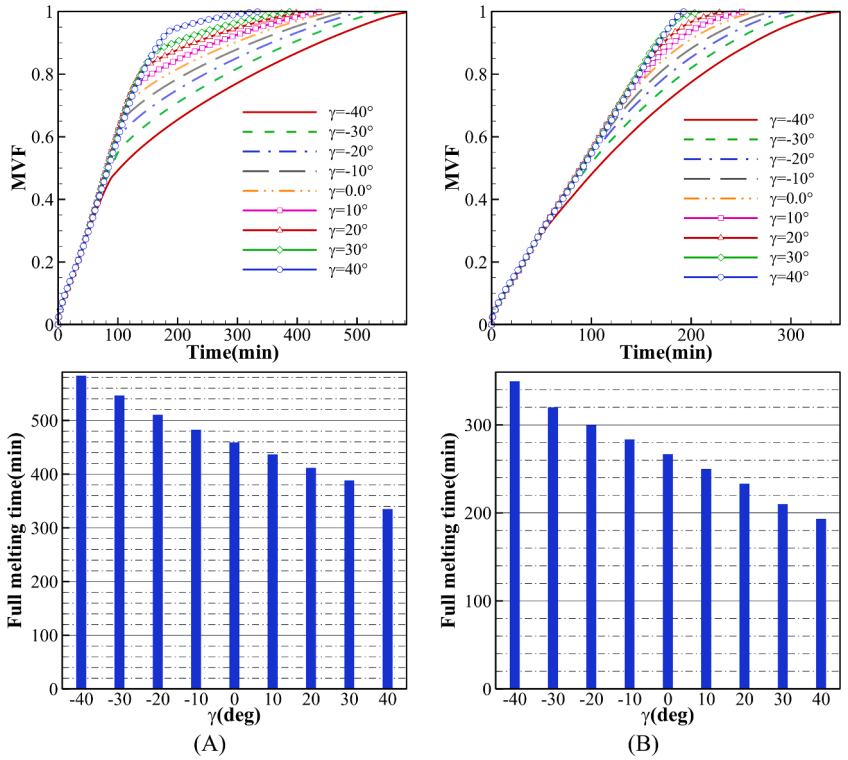

Fig. 7 (a). The effect of angle of the trapezoidal enclosure on the MVF; (A) horizontal arrangement of the hot cylinders, and (B) vertical arrangement of the hot cylinders.

Other positive angles have the increasing trend of lower slop toward $\gamma = 10^{\circ}$, that the time of the whole melting is $t = 250\,min$. This increase in the melting time is seen as the angles of the cavity become negative. For example, the time of melting for the angle, $\gamma = -40^{\circ}$ is around $t = 400\,min$ that is around 150 min more than $\gamma = 40^{\circ}$. This proves the idea that a larger area above the cylinders contributes to more space for the convective term, leading to the shorter whole melting process of the PCM. For the horizontal configuration, Fig. 7 (a) (A), after the primary conductive dominancy period, the reduction in the slope of increasing rate of MVF is more intense than vertical form. In other words, reaching the full melting of PCMs takes longer in the case of horizontal configurations. In this configuration, the total time of melting for $\gamma = -40^{\circ}$ and $\gamma = 40^{\circ}$ is $t = 600\,min$ and $t = 350\,min$, respectively. So, it shows that the maximum difference in the whole melting time between positive and negative angles for horizontal configuration is larger than the vertical one. Caparisoning two horizontal and vertical arrangements for cylinders, vertical form of cylinders lead to less whole melting time of PCM. This was also seen in Fig. 4 (a) and 5 (a). This is the reason for the buoyancy effects, and movement of the melted PCMs from the bottom cylinder added to the higher cylinder's melted PCM, leading to the stronger cells of fluids and a higher rate of melting in the whole area of the cavity.

To compare the MVF of the different cases with the MVF corresponding to $\gamma = 0^{\circ}$, the P_{MVF} is defined as the following:

$$P_{MVF} = \frac{MVF_{\gamma} - MVF_{\gamma=0^{\circ}}}{MVF_{\gamma=0^{\circ}}} \tag{10}$$

Fig. 7 (b) shows the trend of the P_{MVF} by the time for various angles of the trapezoidal cavity at both horizontal and vertical arrangements of the cylinders. As seen, for the negative angle of trapezoidal cavity, the melting rate in the whole cavity is less than the configuration of $\gamma = 0.0^{\circ}$. This is the result of less area of melting above the cylinders in these configurations in comparison to $\gamma = 0.0^{\circ}$. For the positive angles, there is a small positive area of the P_{MVF} at the primary times, and after the formation of the thermal boundary layer and less heat flux, a fall in the P_{MVF} is seen. After this time and empowering of the natural convection, a sharp increase in the positive angle configuration is seen, as there is a larger area above the hot cylinders for the movement of melted PCMs compared to the cavity of $\gamma = 0.0^{\circ}$. It should be mentioned that the total time of melting of the vertical arrangement of cylinders is less than the horizontal one, as the buoyancy effect on the melting process of this arrangement is more than the horizontal one.

6. Effect of the nanoplates dispersed inside the PCM

In this section, the effect of adding different volume fractions of nanoparticles (φ) to the PCM on thermal parameters of the PCM within the cavity is examined. Fig. 8 (a) shows the melting rate of the PCM, streamlines, and velocity field for different time steps when $\varphi = 0.0\%$, 1.0% and 3.0% for the vertical arrangement of the cylinders. It is seen that at the primary times ($t = 2000s$), due to the role of conductive heat transfer, the PCM containing higher nanoparticles ($\varphi = 3.0\%$) experiences more melting. This is the reason for the increment in thermal conductivity of the PCM by nanoparticles. As time passes and more melted PCM cells are created, the natural convection heat transfer term based on the buoyancy effects enhances and leads to the upward movement of the melted PCMs. Two main vortices are formed at this time ($t = 5000s$), and at the next time step ($t = 8000s$) these two vortices combine and make large vorticity next to the cylinders. As the percentage of the mixed nanoparticles inside the pure PCM increases, the density and viscosity of the NePCM increase. So, the more viscose and heavier NePCM demonstrates the lower maximum velocity among the others at later times when the buoyancy force has more influence on the movement of the melted PCM.

The effect of nanoparticles fraction mixed in the PCM on the temperature field of melting PCM in the vertical arrangement of the cylinders is shown in Fig. 8 (b). As seen, at the primary time snap ($t = 2000s$), when the conductive mechanism is dominant, the area around the hot cylinders experiences the highest temperature, and it decreases toward the corner of the cavity. The buoyancy effect helps the melted PCMs move upward, so the area over the upper cylinder has a higher temperature range in the following times. Therefore, it can be concluded that the nanoparticles lightly influence the temperature field during the melting process.

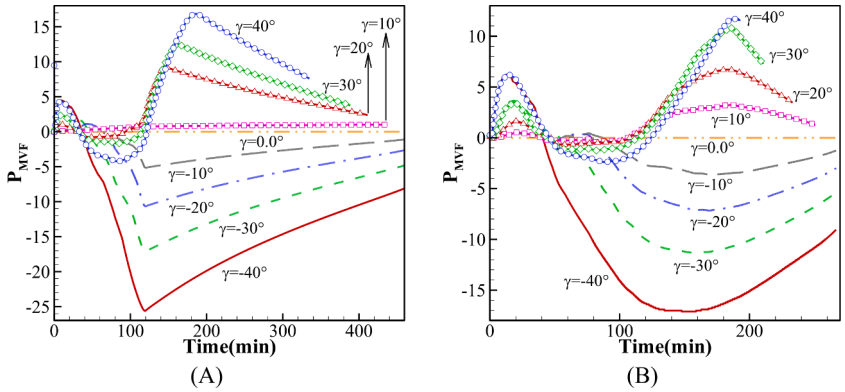

Fig. 7 (b). Time history of the variations percentage of the MVF for different angles of the trapezoidal enclosure; (A) horizontal arrangement of the hot cylinders, and (B) vertical arrangement of the hot cylinders.

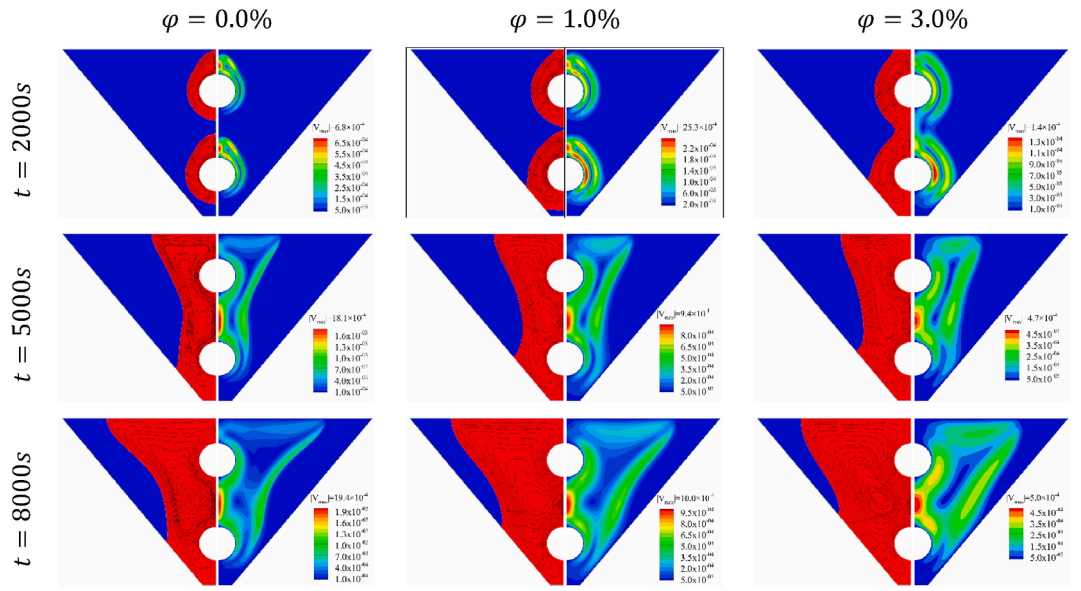

Fig. 8 (a). Dependency of the melting field, streamline patterns, and velocity magnitude field on the mixed nanoparticles percentage inside the PCM for the vertical arrangement of hot cylinders.

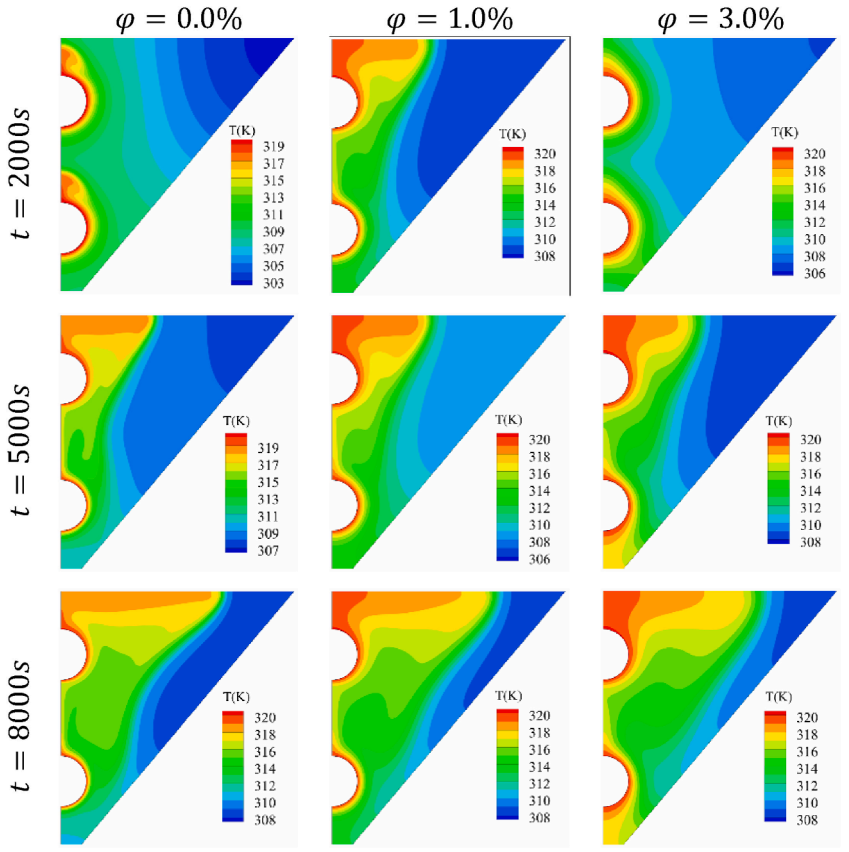

Fig. 8 (b). Dependency of the temperature fields on mixed nanoparticles percentage inside the PCM for the vertical arrangement of hot cylinders.

Fig. 9 (a) illustrates the rate of MVF versus the time and the whole time of melting of PCMs for four different ranges of nanoparticles percentage ($\varphi = 0.0\%, 0.5\%, 1.0\%,$ and 3.0%). It is evident that increasing the percentage of nanoparticles mixed within the PCM contributes to a higher rate of MVF. For example, at the time of $t = 100\,min$, the MVF values for $\varphi = 0.5\%$ and $\varphi = 3.0\%$ are MVF $= 0.45$ and MVF $= 0.62$, respectively. Also, the NePCMs experience less full time of melting. It is worth noting that the full melt-

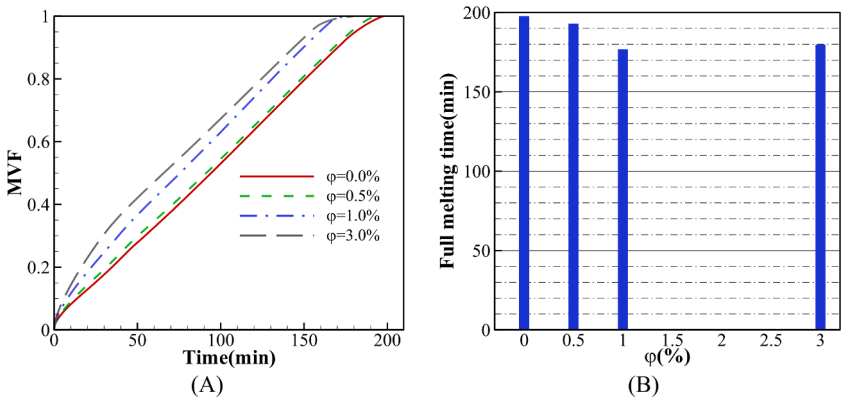

Fig. 9 (a). The effect of mixed nanoparticles percentage on the MVF and full meting time of PCM for vertical arrangement of hot cylinders in the trapezoidal cavity.

ing time of $\varphi = 1.0\%$ is slightly less than $\varphi = 3.0\%$. This could be the reason for better movement of the PCM of $\varphi = 1.0\%$ through the cavity based on the natural convection as it is less dense than the PCM of $\varphi = 3.0\%$.

Fig. 9 (b) shows the variations of the Nusselt number versus time for different percentages of nanoparticles within the NePCM at the vertical arrangement of the hot cylinders. After the sharp decrease of the Nusselt number at the primary time ($t < 20\ min$) due to the formation of the thermal boundary layer, the dominancy of the natural convection contributes to the equivalency between these heat transfer methods, leading to the constant trend of the Nusselt number. The NePCMs with a higher percentage of nanoparticles have a lower melting time, leading to the thermal equilibrium of the liquid melted NePCM with the hot cylinders and sooner fall in the Nusselt number.

7. Conclusion

This study aims to understand the dynamic behavior of phase change process in a trapezoidal thermal energy storage system featuring NePCM with graphite nanoplatelets. The comprehensive investigation into the effects of trapezoidal cavity inclination, nanoparticle concentration, and hot cylinder arrangements on PCM melting rate can lead to valuable insights. The walls of the trapezoidal cavity are fully insulated, and the angle of the trapezoid varies from $\gamma = -40^{\circ}$ to $\gamma = +40^{\circ}$. Thermofluidic characteristics of the melting PCM have been investigated for two arrangements of the hot cylinders and different angles of the trapezoidal cavity. Numerical simulations have been performed based on the enthalpy-porosity approach, and a fixed grid and mesh adoption technique have been employed. The positioning of hot cylinders, whether horizontally or vertically, and the variation of the trapezoidal cavity angle have been shown to exert significant influence on the melting process. The results of this study, aimed at addressing the inquiries introduced in the introduction section, can be succinctly outlined in the following manner:

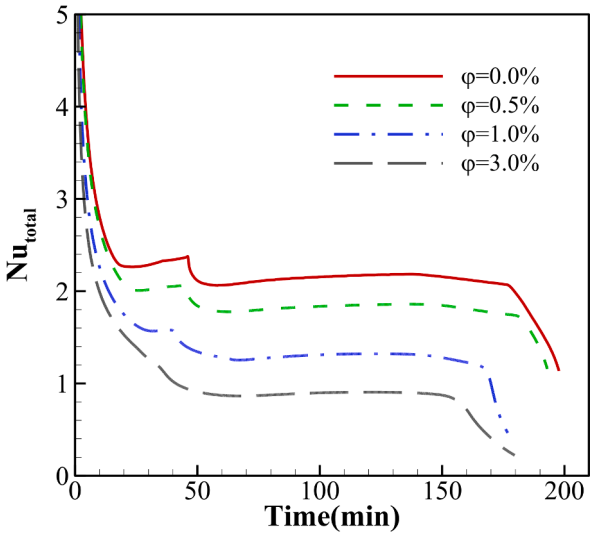

Fig. 9 (b). The variations of the Nusselt number for different percentages of nanoparticles within the NePCM for vertical arrangement of hot cylinders in the trapezoidal cavity.

- For both horizontal and vertical configurations of the cylinders, the PCM has its maximum melting amount at $\gamma = +30^{\circ}$ as the moving area for the melted PCM above the cylinders is more significant than $\gamma = 0.0^{\circ}$ and $\gamma = -30^{\circ}$. Also, the maximum velocity magnitude is seen at this angle for both configurations. In the case of the temperature field, the areas around the cylinder and the top part of the cavities show the highest values. All the cavity configurations and arrangement of cylinders experience a downward trend in heat transfer as the temperature difference between hot cylinders and PCM decreases over time.
- Comparing the arrangement of the cylinders, it shows that the vertical arrangement leads to the lower time of the whole PCM melting. For example, at the cavity angle of $\gamma = 0.0^{\circ}$, the melting time of the PCM in the vertical arrangement is around 45% less than the horizontal one. Among different angles of the trapezoidal cavity ($-40^{\circ} < \gamma < +40^{\circ}$, the longest time of melting is for the angle of $\gamma = -40^{\circ}$, and the shortest time of melting is experienced by the cavity of $\gamma = +40^{\circ}$. So, the cavity angle of $\gamma = +40^{\circ}$ with the vertical arrangement of the cylinders is the best choice in the case of shortest melting ($t = 190\,min$).
- In the case of enhanced PCM by nanoparticles, the melting time decreases compared to the base PCM. The melting time of NePCM of $\varphi = 3.0\%$ is 10% less than base PCM.

Some limitations of this study include the simplified geometry used for this research, which could be replaced with real-world application geometries. Future research could focus on more complex geometries and also investigate the impact of irregular shapes on PCM melting. Also, investigating different cavity geometries and arrangement of the cylinders to find the optimal configurations could be another research area for the future. There could be a parametric study on the variables of this study including concentration, size and type of nanoparticles would provide deeper insights into their effects on the melting process. There could be more experimental investigations for these configurations to have more comprehensive understanding of PCM behavior in practical applications.

CRediT authorship contribution statement

Nidhal Ben Khedher: Conceptualization, Methodology, Writing – original draft, Writing – review & editing. **S.A.M. Mehryan:** Investigation, Methodology, Supervision, Writing – review & editing. **Mohammad Shahabadi:** Conceptualization, Investigation, Validation, Writing – original draft, Writing – review & editing. **Amira M. Hussin:** Conceptualization, Supervision, Writing – original draft, Writing – review & editing. **Abed Saif Alghawli:** Conceptualization, Data curation, Formal analysis, Methodology, Software. **Mohsen Sharifpur:** Funding acquisition, Investigation, Supervision, Writing – original draft, Writing – review & editing.

Declaration of competing interest

The authors declare that they have no conflict of interest.

Data availability

Data will be made available on request.

Acknowledgement

This study is supported via funding from Prince Sattam bin Abdulaziz University project number (PSAU/2024/R/1445).

References

[1] S. Yang, Y. Zhang, Z. Sha, Z. Huang, H. Wang, F. Wang, J. Li, Deterministic Manipulation of heat flow via three-dimensional-Printed thermal Meta-materials for multiple Protection of critical components, ACS Appl. Mater. Interfaces 14 (34) (2022) 39354–39363.
[2] E. Saedpanah, M. Lahonian, M.Z. Malek Abad, Optimization of multi-source renewable energy air conditioning systems using a combination of transient simulation, response surface method, and 3E lifespan analysis, Energy 272 (2023) 127200.
[3] X. Wang, B. Li, D. Gerada, K. Huang, I. Stone, S. Worrall, Y. Yan, A critical review on thermal management technologies for motors in electric cars, Appl. Therm. Eng. 201 (2022) 117758.
[4] Z. Zhu, E. Nadimi, M. Asadollahzadeh, M. Bahari, M. Zare Malek Abad, M. Aliehyaei, Investigation into the effect of multiple line dipoles magnetic field through LS-3 parabolic trough solar system, Appl. Therm. Eng. 235 (2023) 121332.
[5] L. Zhou, F. Meng, Y. Sun, Numerical study on infrared detectors cooling by multi-stage thermoelectric cooler combined with microchannel heat sink, Appl. Therm. Eng. 236 (2024) 121788.
[6] L. Yang, X. Jin, Y. Zhang, K. Du, Recent development on heat transfer and various applications of phase-change materials, J. Clean. Prod. 287 (2021) 124432.
[7] R. Elarem, T. Alqahtani, S. Mellouli, W. Aich, N.B. Khedher, L. Kolsi, A. Jemni, Numerical study of an Evacuated Tube Solar Collector incorporating a Nano-PCM as a latent heat storage system, Case Stud. Therm. Eng. 24 (2021) 100859.
[8] H.A. Nasef, S.A. Nada, H. Hassan, Integrative passive and active cooling system using PCM and nanofluid for thermal regulation of concentrated photovoltaic solar cells, Energy Convers. Manag. 199 (2019) 112065.
[9] N.B. Khedher, S.B. Nasrallah, Three-dimensional simulation of the thermal performance of porous building brick impregnated with phase change material, International Journal of Heat & Technology 32 (1) (2014) 163–169.
[10] W. Hua, L. Zhang, X. Zhang, Research on passive cooling of electronic chips based on PCM: a review, J. Mol. Liq. 340 (2021) 117183.
[11] M.Z. Mahmoud, H.I. Mohammed, J.M. Mahdi, D.O. Bokov, N. Ben Khedher, N.K. Alshammari, et al., Melting enhancement in a Triple-tube latent heat storage system with sloped fins, Nanomaterials 11 (11) (2021) 3153.
[12] H.M.T. Al-Najjar, J.M. Mahdi, D.O. Bokov, N.B. Khedher, N.K. Alshammari, M.J. Catalan Opulencia, et al., Improving the melting duration of a PV/PCM system integrated with different metal foam configurations for thermal energy management, Nanomaterials 12 (3) (2022) 423.
[13] Z. Wang, Y. Diao, Y. Zhao, C. Chen, T. Wang, L. Liang, Visualization experiment and numerical study of latent heat storage unit using micro-heat pipe arrays: melting process, Energy 246 (2022) 123443.
[14] S.L. Tariq, H.M. Ali, M.A. Akram, M.M. Janjua, M. Ahmadlouydarab, Nanoparticles enhanced phase change materials (NePCMs)-A recent review, Appl. Therm. Eng. 176 (2020) 115305.

[15] C. Liu, Z. Rao, J. Zhao, Y. Huo, Y. Li, Review on nanoencapsulated phase change materials: preparation, characterization and heat transfer enhancement, Nano Energy 13 (2015) 814–826.
[16] M. Eslami, F. Khosravi, H.F. Kohan, Effects of fin parameters on performance of latent heat thermal energy storage systems: a comprehensive review, Sustain. Energy Technol. Assessments 47 (2021) 101449.
[17] B. Kamkari, H.J. Amlashi, Numerical simulation and experimental verification of constrained melting of phase change material in inclined rectangular enclosures, Int. Commun. Heat Mass Tran. 88 (2017) 211–219.
[18] Ç. Yıldız, M. Arıcı, S. Nižetić, A. Shahsavar, Numerical investigation of natural convection behavior of molten PCM in an enclosure having rectangular and tree-like branching fins, Energy 207 (2020) 118223.
[19] F. Ahmad, S. Hussain, I. Ahmad, T.S. Hassan, A.O. Almatroud, W. Ali, I.E. Farooq, Successive melting of a phase change material bounded in a finned trapezoidal domain, Case Stud. Therm. Eng. 28 (2021) 101419.
[20] R.D.C. Oliveski, F. Becker, L.A.O. Rocha, C. Biserni, G.E.S. Eberhardt, Design of fin structures for phase change material (PCM) melting process in rectangular cavities, J. Energy Storage 35 (2021) 102337.
[21] Khan MS. Zeeshan, I. Khan, S.M. Eldin, Hira. Numerical solution of heat and mass transfer using buongionro nanofluid model through a porous stretching sheet impact of variable magnetic, heat source, and temperature conductivity, Sci. Prog. 106 (3) (2023) 368504231201542.
[22] Khan I. Zeeshan, S.M. Eldin, S. Islam, M.U. Khan, Two-dimensional nanofluid flow impinging on a porous stretching sheet with nonlinear thermal radiation and slip effect at the boundary enclosing energy perspective, Sci. Rep. 13 (1) (2023) 5459.
[23] Zeeshan n. Heat enhancement analysis of Maxwell fluid containing molybdenum disulfide and graphene nanoparticles in engine oil base fluid with isothermal wall temperature conditions. Waves Random Complex Media.1-15..
[24] M.A. Alomari, K. Al-Farhany, Q.H. Al-Salami, K. Al-Jaburi, F.Q.A. Alyousuf, I.R. Ali, N. Biswas, Magnetohydrodynamic mixed convection in lid-driven curvilinear enclosure with nanofluid and partial porous layer, J. Magn. Magn Mater. 582 (2023) 170952.
[25] M.K. Mondal, D. Kumar Mandal, N. Biswas, N.K. Manna, K. Al-Farhany, A.J. Chamkha, Enhanced magneto-convective heat transport in porous hybrid nanofluid systems with multi-frequency nonuniform heating, J. Magn. Magn Mater. 577 (2023) 170794.
[26] K. Al-Farhany, M.F. Al-dawody, D.A. Hamzah, W. Al-Kouz, Z. Said, Numerical investigation of natural convection on Al2O3–water porous enclosure partially heated with two fins attached to its hot wall: under the MHD effects, Appl. Nanosci. 13 (1) (2023) 555–572.
[27] N.S. Dhaidan, S.A. Kokz, F.L. Rashid, A.K. Hussein, O. Younis, F.N. Al-Mousawi, Review of solidification of phase change materials dispersed with nanoparticles in different containers, J. Energy Storage 51 (2022) 104271.
[28] S. Mehryan, M. Ismael, M. Ghalambaz, Local thermal nonequilibrium conjugate natural convection of nano-encapsulated phase change particles in a partially porous enclosure, Math. Methods Appl. Sci. (2020).
[29] A. Laouer, M. Teggar, E. Tunçbilek, M. Arıcı, L. Hachani, K.A. Ismail, Melting of hybrid nano-enhanced phase change material in an inclined finned rectangular cavity for cold energy storage, J. Energy Storage 50 (2022) 104185.
[30] X. Meng, S. Liu, J. Zou, F. Liu, J. Wang, Inclination angles on the thermal behavior of Phase-Change Material (PCM) in a cavity filled with copper foam partly, Case Stud. Therm. Eng. 25 (2021) 100944.
[31] T. Sathe, A. Dhoble, Experimental investigations of phase change material filled rectangular enclosure with inclined top and side heating mode, J. Energy Storage 32 (2020) 101799.
[32] A.I.N. Korti, H. Guellil, Experimental study of the effect of inclination angle on the paraffin melting process in a square cavity, J. Energy Storage 32 (2020) 101726.
[33] F. Selimefendigil, H.F. Öztop, Mixed convection in a PCM filled cavity under the influence of a rotating cylinder, Sol. Energy 200 (2020) 61–75.
[34] Z.-Q. Zhu, M.-J. Liu, N. Hu, Y.-K. Huang, L.-W. Fan, Z.-T. Yu, J. Ge, Inward solidification heat transfer of nano-enhanced phase change materials in a spherical capsule: an experimental study, J. Heat Tran. 140 (2) (2018).
[35] F.J. Gumir, K. Al-Farhany, W. Jamshed, E.S.M. Tag El Din, A. Abd-Elmonem, Natural convection in a porous cavity filled (35%MWCNT-65% Fe3O4)/water hybrid nanofluid with a solid wavy wall via Galerkin finite-element process, Sci. Rep. 12 (1) (2022) 17794.
[36] H. Bashirpour-Bonab, Investigation and optimization of PCM melting with nanoparticle in a multi-tube thermal energy storage system, Case Stud. Therm. Eng. 28 (2021) 101643.
[37] M. Ghalambaz, S.A.M. Mehryan, A. Hajjar, O. Younis, M.A. Sheremet, M.S. Pour, C. Hulme-Smith, Phase-transition thermal Charging of a Channel-shape thermal energy storage Unit: Taguchi optimization approach and copper foam Inserts, Molecules 26 (5) (2021) 1235.
[38] R.L. Taylor, O.C. Zienkiewicz, The Finite Element Method, Butterworth-Heinemann Oxford, 2013.
[39] O. Schenk, K. Gärtner, Solving unsymmetric sparse systems of linear equations with PARDISO, Future Generat. Comput. Syst. 20 (3) (2004) 475–487.
[40] P. Wriggers, Nonlinear Finite Element Methods, Springer Science & Business Media, 2008.
[41] B. Kim, D. Lee, M. Ha, H. Yoon, A numerical study of natural convection in a square enclosure with a circular cylinder at different vertical locations, Int. J. Heat Mass Tran. 51 (7–8) (2008) 1888–1906.